Supplementary Information

Combined Experimental-Theoretical Study of Electron Mobility-Limiting Mechanisms in $SrSnO_3$

Tristan K. Truttmann[*,1], Jin-Jian Zhou[2], I-Te Lu[2], Anil Kumar Rajapitamahuni[1], Fengdeng Liu[1], Thomas E. Mates[3], Marco Bernardi[*,2], and Bharat Jalan[*,1]

[1]Department of Chemical Engineering and Materials Science, University of Minnesota, Minneapolis, MN 55455, USA

[2]Department of Applied Physics and Materials Science, California Institute of Technology, Pasadena, CA 91125, USA

[3]Materials Department, University of California, Santa Barbara, Santa Barbara, CA 93106, USA

Corresponding Authors

Correspondence should be addressed to TKT (email: trutt009@umn.edu, ORCID: orcid.org/0000-0003-3016-4340) or to MB (bmarco@caltech.edu) or to BJ (email: bjalan@umn.edu, ORCID: orcid.org/0000-0002-7940-0490)

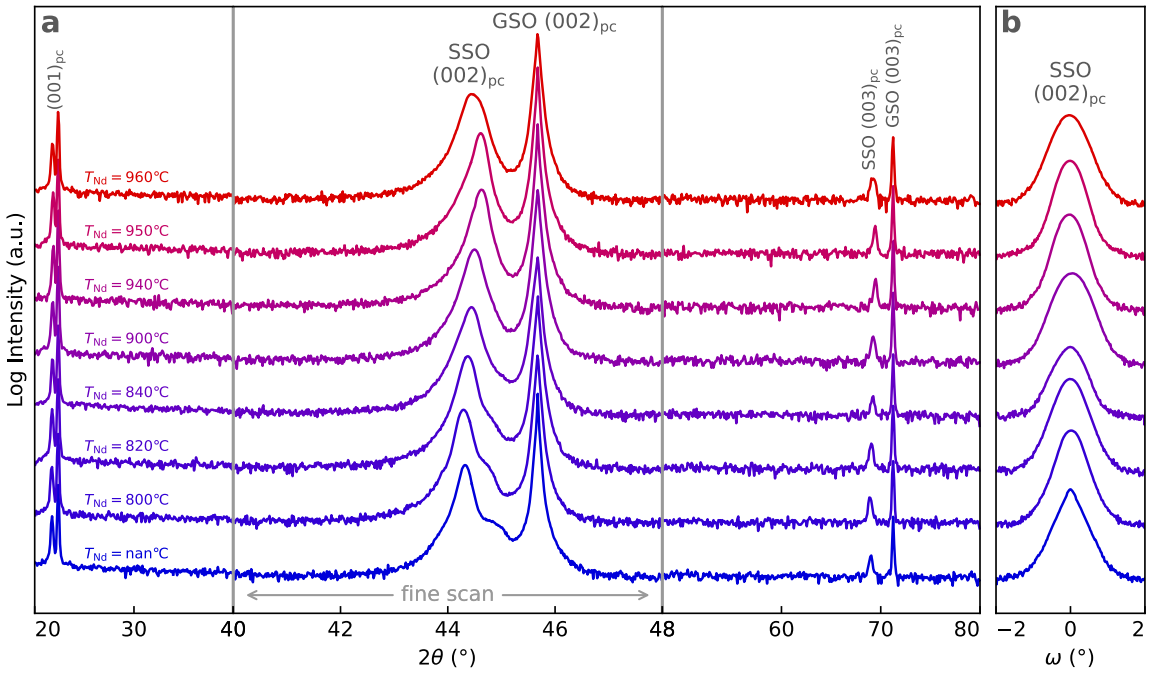

Supplementary Figure 1 | High-resolution X-ray diffraction. The high-resolution specular 2θ-ω coupled scans (**a**) and $Nd_xSr_{1-x}SnO_3$ (SSO) $(002)_{pc}$ rocking curves (**b**) for each of the samples grown on $GdScO_3$ (GSO) $(002)_{pc}$ substrate at different effusion cell temperatures T_{Nd}. These data show that these samples are phase pure and epitaxial. Here, pc refers to pseudocubic.

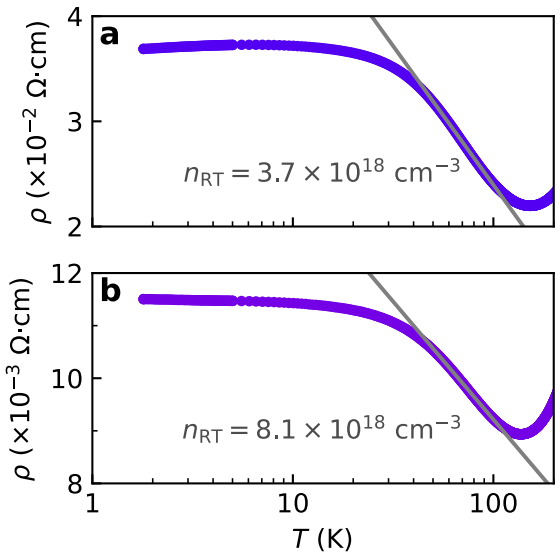

Supplementary Figure 2 | Kondo scattering logarithmic temperature dependence and saturation. The resistivity vs log-scale temperature of $Nd_xSr_{1-x}SnO_3$ films grown at Nd effusion cell temperature T_{Nd} = 820 °C (**a**) and T_{Nd} = 840 °C (**b**). Linear fits are shown for the region with logarithmic temperature dependence.

Supplementary Note 1: SIMS Measurements

To quantify the Nd concentration in the $Nd_xSr_{1-x}SnO_3$ films, we performed dynamic secondary ionization mass spectrometry (SIMS). The SIMS quantification from a previous study on $La_xSr_{1-x}SnO_3$ are shown for reference in Supplementary Figure 3a [1], and the results from this study are shown in Supplementary Figure 3b. Supplementary Figure 3a clearly shows a match of the SIMS and Hall measurements, representing 100% activation of the La dopants. Therefore, it is rather surprising that the Nd concentration in Supplementary Figure 3b was found to be $N_{Nd} = 9.8 \times 10^{19}$ cm^{-3} whereas Hall measurements determined a carrier concentration of $n = 1.6 \times 10^{20}$ cm^{-3}. Naively, this represents 163% dopant activation. Alone, this might be explained by oxygen vacancies, but such a high contribution from oxygen vacancies would be clearly visible as a y-intercept of 6.1×10^{19} cm^{-3} in Fig. 1b. Therefore, we look to other possible explanations to the result in Supplementary Figure 3b.

One major difference between La and Nd is that La has only one abundant isotope, ^{139}La with 99.911% natural abundance, whereas Nd has 7 abundant (> 5%) isotopes spanning 9 atomic mass units. We analyzed the isotope distribution of the five most-abundant Nd isotopes in an implanted sample. These abundances in Supplementary Figure 3c clearly show substantial deviations from the natural abundances, despite specifically requesting natural abundances. Furthermore, we divided the implanted abundances by the natural ones to determine an "enhancement factor" which are shown in Supplementary Figure 3d. This shows the these deviations are systematic, with the masses 143 and below being enhanced, and masses 144 and above being depleted compared to their natural abundances. This can only be explained by the implanter's limited mass resolution, which prevents them from selecting a single isotope for a time proportional to their abundance; instead the implanter sets the mass window somewhere in the middle of the isotope distribution,

and the finite window width accepts many isotopes, albeit with a modified distribution. However, Supplementary Figure 3d shows that the window was not centered at 144, the center of the Nd mass distribution, but was instead centered around 142, the far left of the distribution. The inability of the implanter to supply the natural isotope distribution in addition to the inexplicable low-mass center of the acceptance window degrades our confidence in the implanted standard, which explains the bewildering result in Supplementary Figure 3b. Therefore, we find these SIMS results to be untrustworthy, and we instead rely on the relationship between the carrier concentration and the equilibrium flux at the crucible orifice to infer the dopant activation.

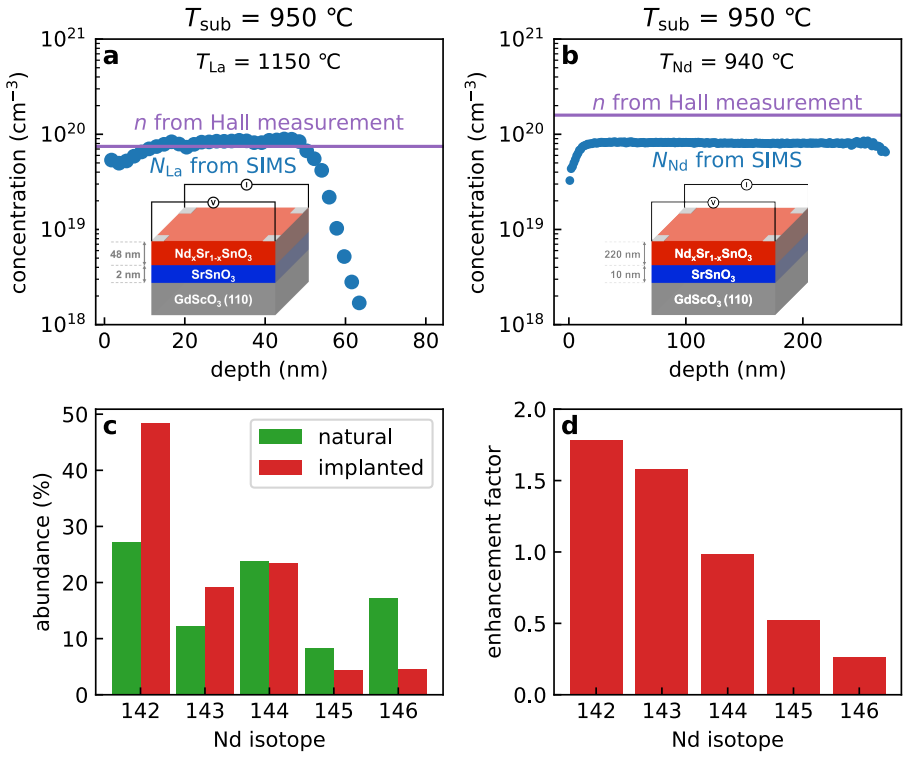

Supplementary Figure 3 | SIMS Depth Profiles and Isotope Abundances. a Lanthanum concentration (N_{La}) of $La_xSr_{1-x}SnO_3$ films determined by secondary ionization mass spectrometry (SIMS) compared to carrier concentration (n) determined by Hall measurements from an earlier publication[1]. **b** The SIMS neodymium concentration (N_{Nd}) determination from this study compared to n determined from Hall measurements. **c** The isotope abundances for the Nd implant compared to natural abundances. **d** The enhancement factor of each Nd isotope.

T_{Nd} (°C)	$\Delta\omega_{sub}$	$\Delta\omega_{film}$
960	0.019°	0.551°
950	0.010°	0.453°
940	0.011°	0.475°
900	0.020°	0.591°
840	0.033°	0.501°
820	0.011°	0.486°
800	0.017°	0.449°
OFF	0.007°	0.286°

Supplementary Table 1 | Rocking Curve FWHM. The rocking curve full widths at half maximum (FWHM) are tabulated for each $GdScO_3$ substrate ($\Delta\omega_{sub}$) and its corresponding $Nd_xSr_{1-x}SnO_3$ films ($\Delta\omega_{film}$).

Supplementary References

1 Truttmann, T., Prakash, A., Yue, J., Mates, T. E. & Jalan, B. Dopant solubility and charge compensation in La-doped $SrSnO_3$ films. *Applied Physics Letters* **115**, 152103, doi:10.1063/1.5119272 (2019).